Materials Chemistry and Physics 259 (2021) 124065

Contents lists available at ScienceDirect

Materials Chemistry and Physics

journal homepage: www.elsevier.com/locate/matchemphys

Ab initio comparative study of the magnetic, electronic and optical properties of AB_2O_4 (A, B= Mn, Fe) spinels

V.S. Zhandun *, A.V. Nemtsev

Kirensky Institute of Physics, Federal Research Center, Krasnoyarsk Science Centre, Siberian Branch of the Russian Academy of Sciences, 660036, Krasnoyarsk, Russia

HIGHLIGHTS

- The effect of the cation's site on the properties of the spinels is studied.
- The electronic and structural properties of spinels depend on the composition.
- The exchange constants of the spinels are estimated.
- The abrupt decrease of the FeMn2O4 spinel total magnetization under pressure is predicted.

ARTICLE INFO

Keywords:
Ab initio calculations
Spinel
Magnetic and electronic properties
Optical properties
Inverse structure
Manganese and iron oxides

ABSTRACT

The comparison of the magnetic, electronic, and optical properties of the spinel transition-metal oxides AB_2O_4 (A, B = Fe, Mn) and their relationship with the structure and composition were studied within DFT-GGA + U approximation. The spinels were considered both in the normal and inverse structure. We have found that regardless of composition and structure, the studied spinels are ferrimagnetic with antiparallel magnetic moments on A- and B-site cations. Electronic and structural properties of spinels depend on the composition: $FeMn_2O_4$ has a tetragonal structure and half-metallic properties; however, in the inverse $FeMn_2O_4$, the bandgap opens for the spin-up channel. $MnFe_2O_4$ is a cubic insulator with a bandgap of about 1.5 eV, which decreases in the inverse structure. The superexchange constants estimate within the simple indirect coupling model and have values close to the experimental ones. The total magnetization of $FeMn_2O_4$ is drop-down to zero under hydrostatic pressure above 60 GPa due to the strong dependence of the magnetic moment of octahedral manganese ion on the pressure. The microscopic mechanisms of the relationship between the structure, composition and properties are studied.

1. Introduction

The transition metal-containing oxides with the spinel structure are of great importance, as fundamental as well as applied, due to a wide range of the potential applications of their physical and chemical properties. Spinels exhibit a lot of exciting properties such as frustrated antiferromagnetism, multiferroics, spintronics, spin-orbital liquids, and orbital glass behavior [1–6]. The properties of spinels can vary as with the crystal structure as well as the chemical composition. The spinels can be found in two structural modifications: normal spinel and inverse spinel. The crystal structure of normal spinel has general configuration $A^{2+}B^{3+}{}_2O_4$, where bivalent A^{2+} and trivalent B^{3+} are tetrahedrally and octahedrally coordinated cations, respectively. An inverse spinel is an alternative arrangement where the A-site ions and half of the B-site ions switch places. Inverse spinels have the chemical formula $B^{3+}(A^{2+}B^{3+})O_4$, where the bivalent A^{2+} and half of the trivalent B ions occupy octahedral sites, and the other trivalent B ions are on tetrahedral sites.

To study the role of the structure and the effect of the type (Fe and Mn ions) and position (A- and B-sites) of magnetic ions in the structure, we have performed ab initio calculation and comparison of the magnetic, electronic and optical properties of the $FeMn_2O_4$ and $MnFe_2O_4$ spinel oxides in two structural types (normal spinel and inverse spinel). The AB_2O_4 (A, B=Fe, Mn) spinels are well-studied ferrimagnetic materials with antiferromagnet interaction between magnetic ions at positions A and B [7–14]. $MnFe_2O_4$ is a ferromagnetic semiconductor with a bandgap of 2.03 eV [10]. At room temperature, $MnFe_2O_4$ has a cubic

* Corresponding author.
E-mail addresses: jvc@iph.krasn.ru, jandun0812@gmail.com (V.S. Zhandun).

https://doi.org/10.1016/j.matchemphys.2020.124065
Received 10 March 2020; Received in revised form 26 October 2020; Accepted 15 November 2020
Available online 23 November 2020

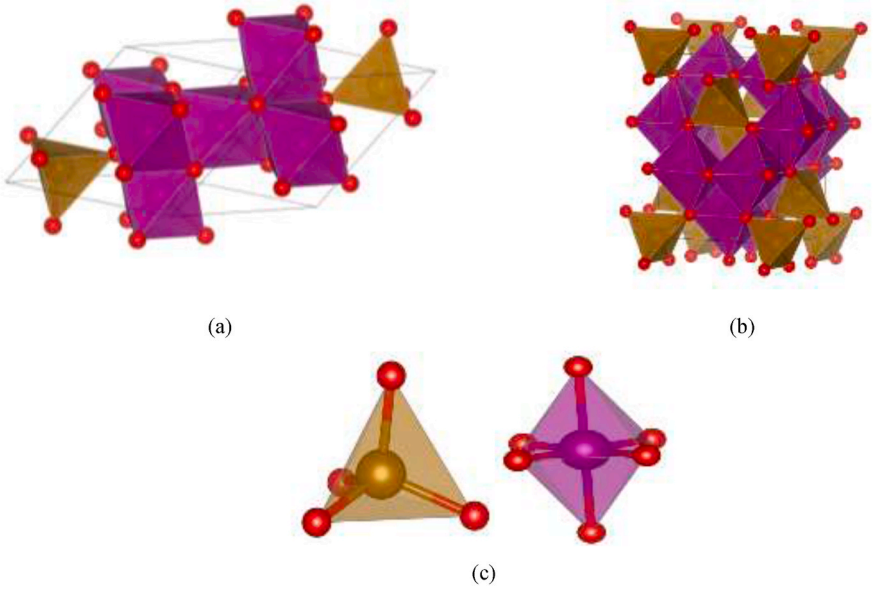

Fig. 1. Crystal structure of the cubic normal spinel (a) and the tetragonal normal spinel (b); local environment of A^{2+} and B^{3+} cations (c). Oxygen tetrahedra are shown by gold color, oxygen octahedra are shown by the purple color. (For interpretation of the references to color in this figure legend, the reader is referred to the Web version of this article.)

structure with a small deviation from the normal spinel structure [15, 16]. $MnFe_2O_4$ shows fascinating properties for research, such as high saturation magnetization (M_s~83 emu/g at 300 K), high chemical stability, and low Curie temperature among spinel ferrites [7]. $FeMn_2O_4$ is a ferrimagnetic half-metal compound; however, when the spinel has the inverse structure, the system becomes a semiconductor, with an insignificant bandgap, which was also found experimentally [13,17]. At room temperature $FeMn_2O_4$ has a tetragonal structure $I4_1/amd$ [13,18] with the magnetic moments $\mu_{Mn} = 3.1\ \mu_B$, $\mu_{Fe} = 4.3\mu_B$ [8]. Despite the many papers devoted to the ferrite and manganite spinels, there are no comparative investigations of the properties of the AB_2O_4 (A, B= Mn, Fe) spinels in the dependence on the structure and the cation location. However, such a study is of interest because a comparison of two compounds of the same composition, but with a different arrangement of ions in the structure, will reveal the relationship of the desired properties with the crystal structure and the local environment of magnetic species. Therefore in the present paper, we study the dependence of the electronic, magnetic, and optical properties on the location and type of A- and B-site cations, and the microscopic mechanisms of this dependence.

The paper is organized as follows. In Sec. II, we give a short description of the computational details, in Sec. IIIA and IIIB, the comparison of magnetic, optic, and electronic properties of the normal and inverse spinels are reported. In the last Section, we make conclusions.

2. Calculation details

All ab initio calculations presented in this paper are performedusing the Vienna ab initio simulation package (VASP) [19] withprojector augmented wave (PAW) pseudopotentials [20]. Thevalence electron configurations $3d^64s^2$ and $3d^54s^2$ were taken for Fe and Mn ions and$3s^23p^4$ for O ions. The calculations are based on the density-functional theory, where the exchange-correlation functional is chosen within the Perdew-Burke-Ernzerhoff (PBE) parameterization [21], and the generalized gradient approximation (GGA) hasbeen used. Throughout all calculations, the plane-wave cutoff energy 500 eV is used. The Brillouin-zone integration is performed on the 8 x 8 x 8 Monkhorst-Pack mesh of special points [22]. As known, the underestimating of the bandgap of transition metal compounds is a lack of density functional theory (DFT) approach. To overcome this problem,

Table 1
The calculated lattice parameters (Å), magnetic moments μ (μ_B), and number of d-electrons on transition metal ion N_{el}. of $MnFe_2O_4$ и $FeMn_2O_4$ normal spinels

	a; c	A-site		B-site	
		μ	N_{el}	μ	N_{el}
$FeMn_2O_4$	5.97; 8.95	−4.13	6.0	4.25	4.9
$MnFe_2O_4$	8.58; 8.58	−4.48	4.9	4.30	5.9

Hubbard repulsion U is often taking into account within the GGA + U scheme. In our calculations, GGA + U calculations were performed within Dudarev's approximations [23] with U = 3 eV and U = 4.5 eV for Mn and Fe ion, correspondingly (following Ref. [24]).

3. Results and discussion

3.1. Normal spinel

At room temperature, the oxide $MnFe_2O_4$ has a normal spinel structure AB_2O_4 (Fig. 1a) with an fcc unit cell (space symmetry group $Fd\bar{3}m$). In turn, oxide $FeMn_2O_4$ crystallizes in the tetragonal (or pseudocubic) $I4_1/amd$ structure (Fig. 1b). In the structure of the normal spinel, bivalent A-site cations are in the tetrahedral environment of oxygen ions, and trivalent B-site cations are surrounded by six oxygen ions located at the vertices of the octahedron. The geometry of both compounds structures was fully optimized within GGA + U for the cubic and tetragonal phases. We have obtained that the ground state for $FeMn_2O_4$ is the tetragonal phase, while the $MnFe_2O_4$ spinel has the cubic phase as the most energy favorable state. However, the energy difference between the tetragonal and cubic phases is tiny (~100K). We should notice that only the account of Hubbard U makes the cubic phase favorable in $MnFe_2O_4$.

Calculated optimized lattice parameters are shown in Table 1. The obtained values are close to the experimental lattice parameter of $MnFe_2O_4$: a = 8.51 [25] and $FeMn_2O_4$: a = b = 5.91 Å, c = 8.91 [13]. We also evaluated the bond lengths inside the oxygen tetrahedrons and octahedrons which are: $d_{Fe\text{-}O} = 1.94$ Å, $d_{Mn\text{-}O} = 2.04$ Å for $FeMn_2O_4$ normal spinel and $d_{Mn\text{-}O} = 1.9$ Å, $d_{Fe\text{-}O} = 2.07$ Å for $MnFe_2O_4$ normal spinel, correspondingly. As seen, in both compounds, the distances

Table 2
The different ordering of magnetic moments on transition-metal ions of $MnFe_2O_4$ и $FeMn_2O_4$ normal spinels.

	Cubic structure	Tetragonal structure
1	↑↓↑↑↑↑	↓↓↓↑↑↑↑↑↑↑
2	↑↑↑↑↑↑	↑↑↑↑↑↑↑↑↑↑
3	↑↓↑↑↓↑	↑↓↑↑↓↑↓↑↓↑
4	↓↓↑↑↑↑	↓↓↓↑↑↑↑↓↓↓
5	↑↑↑↓↑↓	↑↑↑↑↑↑↑↓↓↓
6	↑↑↑↓↑↑	↑↑↓↓↑↑↓↑↑↓
7	↑↓↑↑↑↓	↑↑↑↑↑↓↑↓↑↓

Table 3
The total energies (eV) of $MnFe_2O_4$ и $FeMn_2O_4$ normal spinels with different magnetic ordering in the cubic and tetragonal structure.

Number of ordering type	$MnFe_2O_4$		$FeMn_2O_4$	
	Cubic structure	Tetragonal structure	Cubic structure	Tetragonal structure
1	−109,080	−110,176	−113,278	−114,396
2	−108,167	−108,179	−112,483	−112,642
3	−109,590	−109,589	−113,733	−113,803
4	−110,178	−109,271	−114,388	−113,600
5	−109,305	−109,246	−113,604	−113,613
6	−108,647	−109,128	−112,971	−113,816
7	−108,682	−109,298	−113,516	−113,814

inside the octahedrons are much larger than the distances inside the tetrahedrons. Besides, in $MnFe_2O_4$, the distances inside octahedrons are larger than ones in $FeMn_2O_4$, and vice versa in $FeMn_2O_4$, the distances inside the tetrahedrons are slightly larger than ones in $MnFe_2O_4$. So, the covalency of Mn–O bonds is higher than the covalency of Fe–O bonds.

To obtain the theoretical magnetic ground state, we have considered a few possible magnetic structures with the different directions of magnetic moments on the magnetic species (see Table 2). In Table 3 the total energies of the different magnetic states of $MnFe_2O_4$ и $FeMn_2O_4$ are given for cubic and tetragonal phases. As can be seen, in the most energy favorable magnetic state, the magnetic moments on A- and B-site cations has antiparallel ordering, i.e., both compounds are ferrimagnets. Magnetic moments of the Mn and Fe ions in both spinels are close to each other (μ~4–4.5 μ_B); however, the Mn magnetic moment is slightly larger than Fe magnetic moment regardless of the position in the structure. The magnetic moment of the Mn ion in the tetrahedral position is higher than the magnetic moment of manganese in the octahedral position; for the Fe ion, the situation is opposite for it, which is related to the difference in the bond covalence. The large values of magnetic moments indicate the d-electrons of the Mn and Fe ions are in the high-spin state.

The density of states (Fig. 2) shows that the electronic properties of two spinels are also different. The $FeMn_2O_4$ shows the half-metal behavior as within GGA as well within the GGA + U approach: the spin-up electrons are on the Fermi energy indicating the metallic character of spin-up channel, while spin-down states have a wide bandgap approximately 4.0 eV. The $MnFe_2O_4$ is an insulator with the bandgaps in both spin-up and spin-down channels. Notice, the spin-down bandgap in $MnFe_2O_4$ appears only when Hubbard U is taking into account: without Hubbard U the compound is the half-metal as $FeMn_2O_4$. To find out the role of U on different 3d metals, we have calculated the DOSes of the $MnFe_2O_4$ with and without Hubbard's U on Fe and Mn ions. As seen, turn on Hubbard's U on only tetrahedral Mn ion shifts the spin-down electronic states from Fermi energy; however, the bandgap does not appear. The turn-on the Hubbard's U on octahedral Fe ion, on the contrary, opens the small bandgap. This indicates the more crucial role of the strong electron correlations of the octahedrally coordinated ion in the studied compound. Also as seen from Fig. 3, in both compounds d-electrons of Fe are localized at the energy about −8 eV, whereas d-electrons of Mn ion are delocalized in the wide energy range of [-6;0] eV,

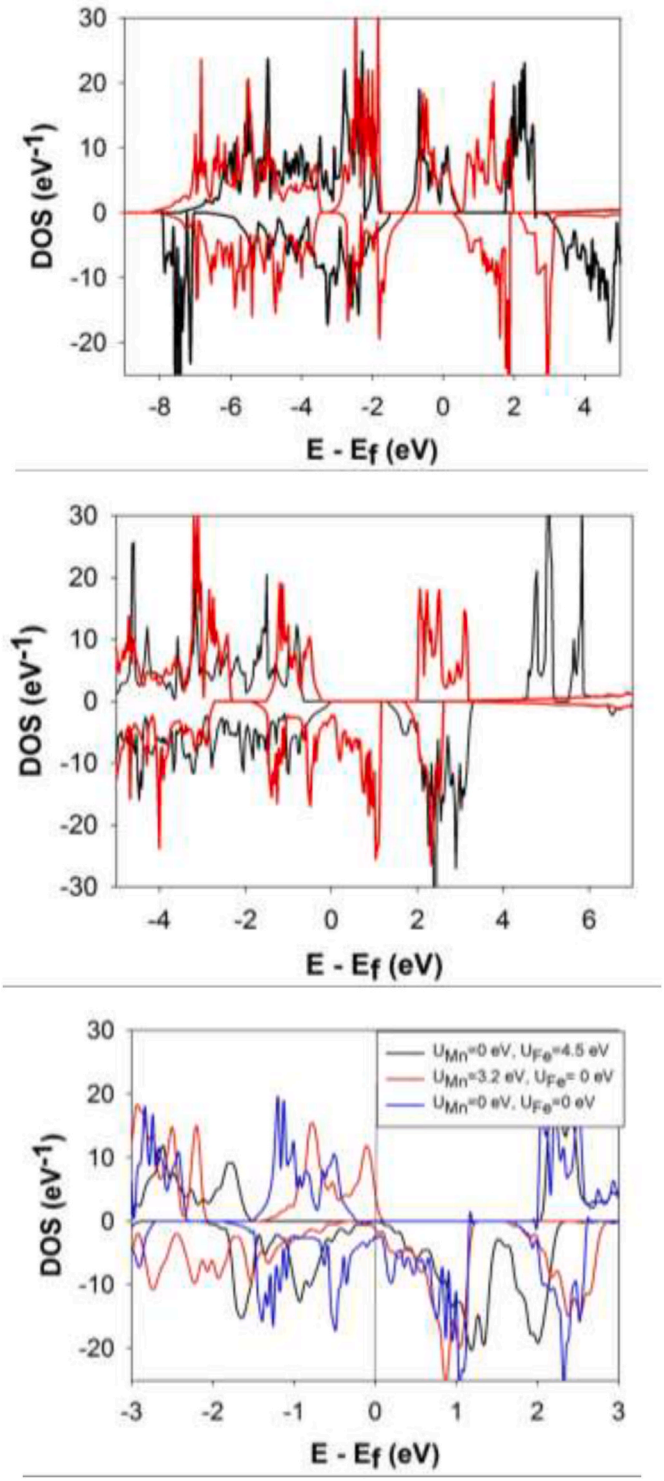

Fig. 2. DOS of normal $FeMn_2O_4$ (a) and $MnFe_2O_4$ (b). Black line – GGA + U, red line – GGA. Panel (c) shows the dependence of DOS of the normal spinel $MnFe_2O_4$ on the different Hubbard's U. The zero on the energy axis is the Fermi energy. Negative values of DOS correspond to the spin-down states. (For interpretation of the references to color in this figure legend, the reader is referred to the Web version of this article.)

where they have strong hybridization with p-electrons of oxygen. In $FeMn_2O_4$, the majority spin state d-electrons of Mn are hybridized near the Fermi energy with d-electrons of Fe ion.

The comparison of the band structures of $FeMn_2O_4$ and $MnFe_2O_4$ spinels are given in Fig. 4. The bands were classified following their

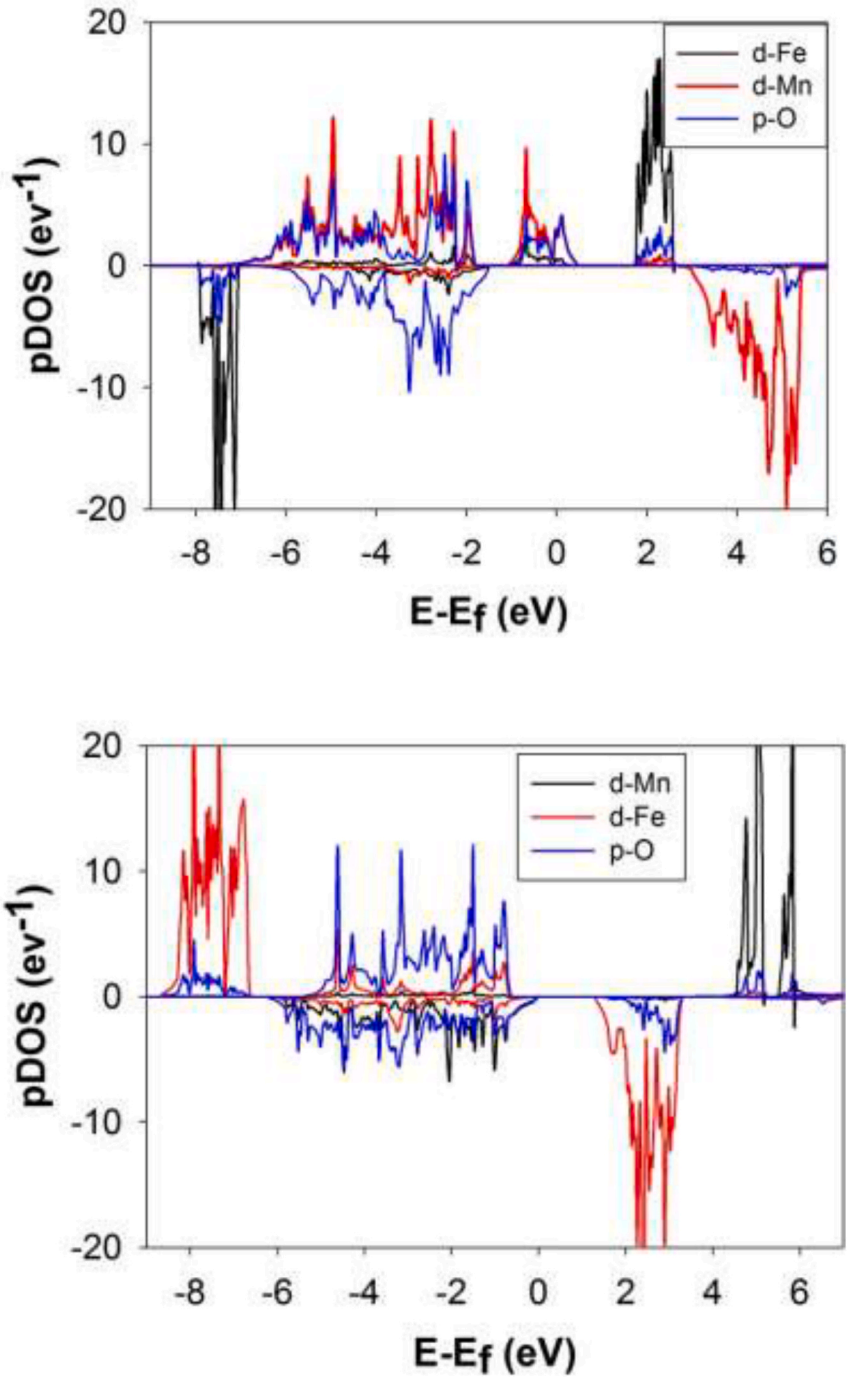

Fig. 3. Projected d- and p-DOS of Mn, Fe, and O ions in (a) $FeMn_2O_4$ (b) $MnFe_2O_4$ normal spinels. The zero on the energy axis is the Fermi energy. Negative values of DOS correspond to the spin-down states.

symmetries in the point Γ of the Brillouin zone. As seen, the band structures differ significantly. In the half-metal $FeMn_2O_4$, the majority spin T2g bands cross the Fermi energy, while minority spin bands have a large energy gap of about 4 eV. Vice versa, dielectric spinel $MnFe_2O_4$, has the direct bandgap for both channels: the minimum of conductive band and maxima of valence band are located in Γ-point. The calculated bandgap is close to the experimental ones [10,26]. It is about 3 eV for the spin-up states, while the bandgap of spin-down states is much smaller, about 1.5 eV. The first empty band with a majority spin (A1g) is formed by s-states, which explains its pronounced dispersion dependence in the Brillouin zone. The eg-states of an iron ion with an admixture of p-states of O ions form the first valence bands. In the case of minority spins, the first empty band (T2g) is formed from the t2g-states of Fe. The first bands filled with minority spins closest to the Fermi energy are formed by the t2g-states of the Mn ion with an admixture of the p-states of the O ions.

As known [27] in spinels with magnetic species on the A- and B-sites, the exchange interaction between tetrahedral and octahedral sublattices stronger than within sublattice. In the normal spinel, the superexchange between tetrahedral and octahedral ions is carried out through intermediate oxygen ions. To estimate the superexchange interactions in $FeMn_2O_4$ and $MnFe_2O_4$ spinels, we used a simple indirect coupling model [28] based on the theory of the superexchange interaction of Anderson [29], and Zavadskii [30]. Within the indirect coupling model,

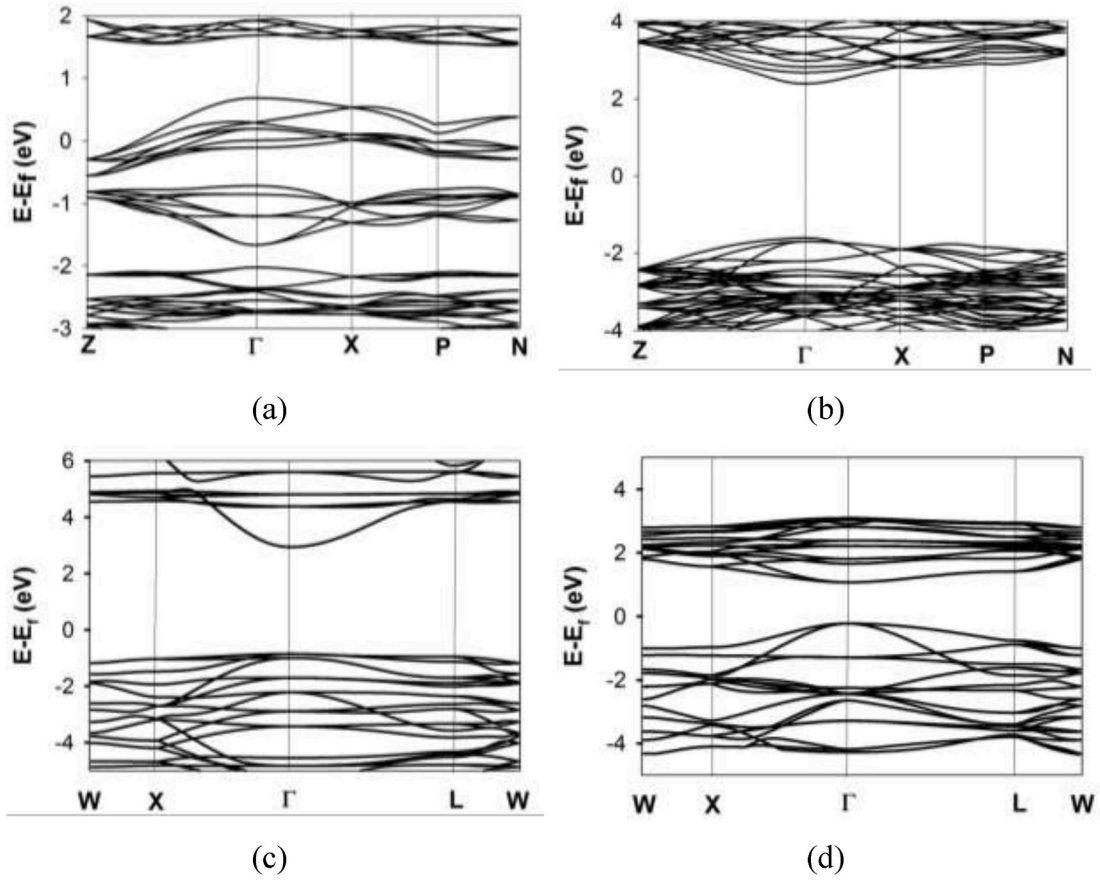

Fig. 4. Band structures of the normal spinels: (a), (b) –$FeMn_2O_4$, (c), (d) – $MnFe_2O_4$. Zero corresponds to the Fermi energy.

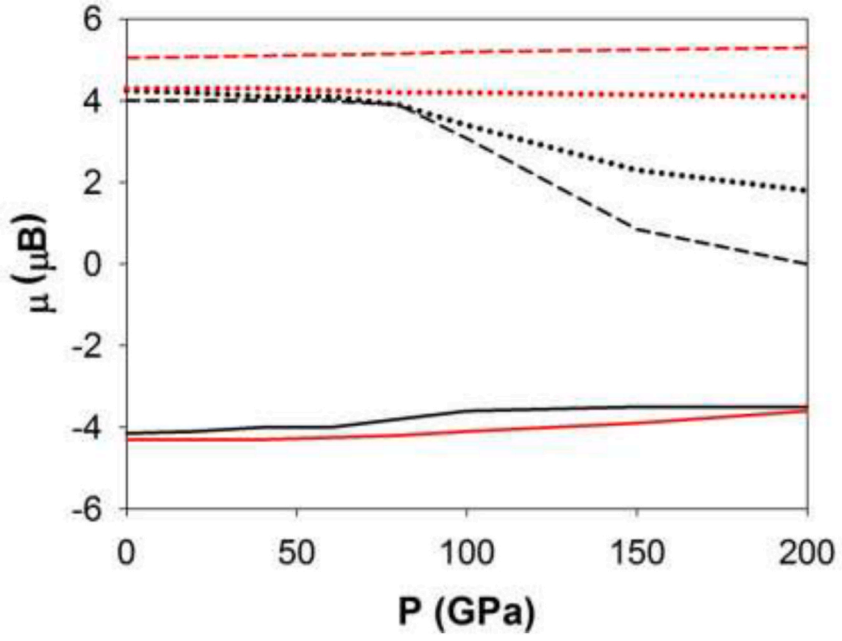

Fig. 5. Pressure dependence of the magnetic moments of A- (solid line) and B-site cations (dashed line) and total magnetization (dotted line) in $FeMn_2O_4$ (black line) and $MnFe_2O_4$ (red line) spinels. (For interpretation of the references to color in this figure legend, the reader is referred to the Web version of this article.)

the structure of the crystal can be characterized by the following integrals of the indirect exchange coupling concerning occupations of individual cation orbitals and symmetries of the lattice of indirect couplings $J_{ij,}$ where i and j are the numbers of nonequivalent crystallographic positions for magnetic ions.

The expressions for the exchange integrals between A- and B-site cations within the indirect coupling model have the following forms for $FeMn_2O_4$ and $MnFe_2O_4$ spinels, correspondingly:

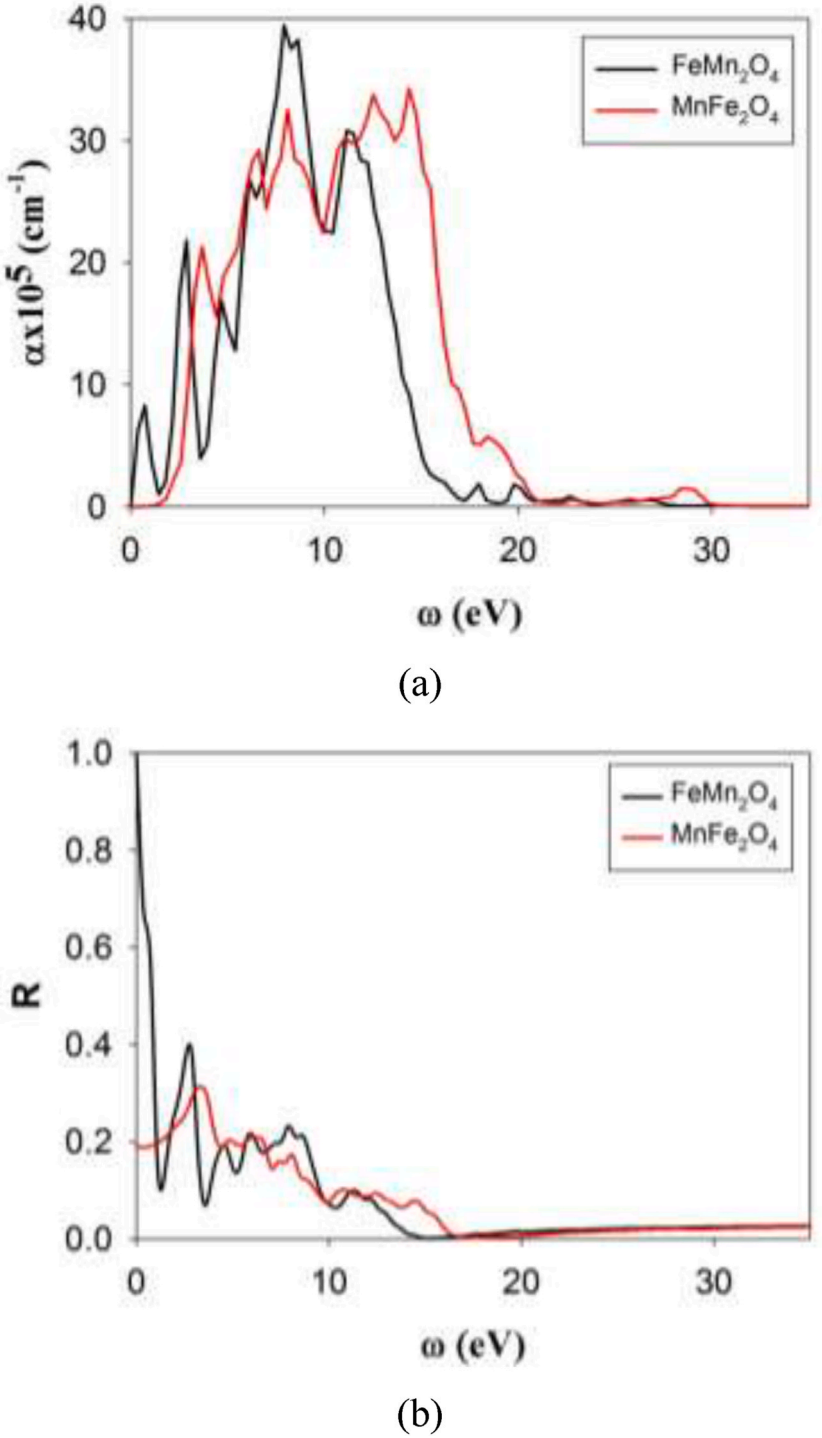

Fig. 6. The comparison of the absorption (a) and reflection (b) spectra of the normal $FeMn_2O_4$ (black line) and $MnFe_2O_4$ (red line) spinels.

$$J_{Fe-Mn} = -\frac{1}{24}a\{(b(U_{Mn} + U_{Fe} - J_{Mn}^{6H}) + 3c(U_{Mn} + U_{Fe})\} \quad (1)$$

$$J_{Mn-Fe} = -\frac{4}{75}a(2b + 3c)U_{Fe} \quad (2)$$

where $U(Mn^{2+}) = 7$ eV, U $(Fe^{2+}) = 6.5$ eV, U $(Mn^{3+}) = 8.5$ eV and U $(Fe^{3+}) = 8$ eV are the cation-ligand excitation energy; a, *b* and *c* are the electron transfer parameters being squares of A and B ligand-cations intermixing coefficients for the σ and π coupling, respectively (the values of these parameters are $a = 0.08$, $b = 0.02$ and $c = 0.01$); $J_{Mn}^{au} = 3$ eV – intraatomic exchange integral [28–30]. The calculated exchange integrals are $J_{Fe\text{-}Mn} = -2{,}38$ meV (~26.2 K) and $J_{Mn\text{-}Fe} = -2{,}1$ meV (~23 K) for $FeMn_2O_4$ and $MnFe_2O_4$ spinel, correspondingly. One can see that Fe–Mn superexchange integrals in both compounds are antiferromagnetic in agreement with the results of our ab initio calculations and experimental data [7,8]. Also notice, that both Fe–Mn superexchange integrals are weak due to the superexchange couplings between magnetic species on the A- and B-sites. Obtained values are comparable with the experimental values: $J_{AB} = 22.7$ K obtained from nuclear magnetic resonance [7] and $J_{AB} = 19.1$ K as measured from magnon dispersion [31]. We also have estimated the exchange between B-site cations in

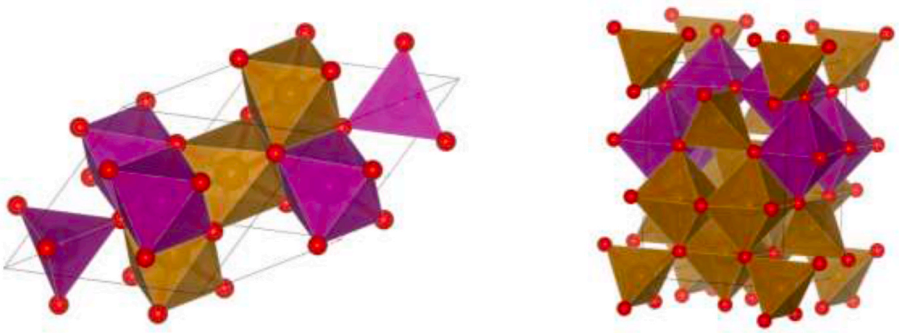

(a) (b)

Fig. 7. The crystal structure of the cubic inverse spinel (a) and the tetragonal inverse spinel (b). Oxygen tetrahedra are shown by gold color, oxygen octahedra are shown by the purple color. (For interpretation of the references to color in this figure legend, the reader is referred to the Web version of this article.)

Table 4
The calculated lattice parameters (Å), magnetic moments μ (μ_B), and number of d-electrons on transition metal ion N_{el} of $MnFe_2O_4$ и $FeMn_2O_4$ inverse spinels

	a; c	A-site		B-site		B-site	
		μ	N_{el}	μ	N_{el}	μ	N_{el}
$Mn(MnFe)O_4$	6.00; 9.06	4.55	4.9	4.00	4.8	−4.22	5.8
$Fe(FeMn)O_4$	8.60; 8.60	4.00	5.8	−4.31	5.7	−4.34	5.0

both compounds, and they turned out to be three times less than the exchange between A- and B-site cations: $J_{Mn\text{-}Mn} = -0{,}8$ meV (~9.0 K) and $J_{Fe\text{-}Fe} = -0{,}7$ meV (~7.5 K) for $FeMn_2O_4$ and $MnFe_2O_4$ spinel, correspondingly.

We also have studied the pressure dependence of the A- and B-sites magnetic moments in both normal spinels (Fig. 5). In cubic $MnFe_2O_4$, the dependence of magnetic moments of both cations on the pressure is weak. In the tetragonal $FeMn_2O_4$, the pressure dependence of Fe magnetic moment (tetrahedral A-site) is also weak, but the Mn magnetic moment (octahedral B-site) drops sharply with increasing pressure in the range of [60–120] GPa. This results in the sharp decrease of the total magnetization down to zero in $FeMn_2O_4$ under pressure. As known, the destruction of the magnetic moments process is highly correlated with the interatomic bond length and bond population distributions. In Mn_2FeO_4, the smooth reduction of bond length between Mn–O and Fe–O ions under pressure results in the smooth decrease of the Mn and Fe magnetic moments. Vice versa, in $FeMn_2O_4$, the distances between Mn–O ions experiencing a sharp decrease at the pressure in the range of [60–120] GPa, while the Fe–O distance in tetrahedra, although also decreases, is more smoothly. It is such a sharp decrease in the Mn–O bond length under applied pressure that leads to sharp destruction of the magnetic moment of the Mn ion.

The comparison of the calculated optical absorption and reflectance of the normal spinel is shown in Fig. 6. The shape of the absorption spectra of both spinels is similar. However, there are some distinctions. At first, the absorption band of $MnFe_2O_4$ is wider than in $FeMn_2O_4$ due to the occupied electronic states are more extended by energy. Secondary, $FeMn_2O_4$ has an absorption peak at low frequencies (~0.7 eV) due to the metal character of the spin-up channel, whereas in the $MnFe_2O_4$, the absorption coefficient is zero in the low-frequency range due to the presence of a bandgap with a width of about 1.5 eV $FeMn_2O_4$ has two absorption peaks: at 0.7 and 2.9 eV (IR and visible range), related to the transitions between states near the Fermi energy, and a large wide absorption band in the range from ~3.6 eV to ~17.2 eV with three pronounced peaks in it: at 4.7 eV, 7.9 eV and 11.1. eV. This wide absorption band is related to the transitions from valence states lying below −2 eV (Fig. 2a). In $MnFe_2O_4$ the wide absorption band is in the range from ~1.4 eV to ~20.1 eV with several pronounced peaks in the

Table 5
The different ordering of magnetic moments on transition-metal ions of $MnFe_2O_4$ и $FeMn_2O_4$ inverse spinels.

	Cubic structure	Tetragonal structure
1	↑↑↑↑↑↑	↑↑↑↑↑↑↑↑↑↑↑↑
2	↑↑↑↓↑↓	↑↑↑↑↓↓↓↓↓↓↓↓
3	↑↑↑↑↓↓	↑↑↓↑↓↑↓↑↓↑↓↑
4	↑↑↓↓↑↑	↑↑↑↑↓↓↓↓↑↑↑↑
5	↑↓↑↑↑↑	↑↑↑↑↑↑↑↑↓↓↓↓
6	↓↓↑↑↓↓	↑↑↓↓↑↑↓↓↑↑↓↓
7	↑↑↓↓↓↓	↑↑↑↑↑↓↑↓↑↓↑↓

Table 6
The total energies (eV) of $MnFe_2O_4$ и $FeMn_2O_4$ inverse spinels with different magnetic ordering in the cubic and tetragonal structure.

Number of ordering type	$MnFe_2O_4$		$FeMn_2O_4$	
	Cubic structure	Tetragonal structure	Cubic structure	Tetragonal structure
1	−109,139	−108,741	−112,648	−112,401
2	−109,273	−110,118	−112,702	−113,632
3	−109,069	−110,100	−113,714	−110,125
4	−109,898	−109,922	−112,763	−109,911
5	−109,925	−110,054	−112,645	−110,054
6	−109,957	−110,031	−112,644	−110,029
7	−110,148	−109,960	−113,568	−109,941

UV range: 3.7 eV, 6.4 eV, 8.1 eV, 12.6 eV and 14.4 eV. The reflectivity spectra also have differences. So, in half-metal $FeMn_2O_4$ the reflectance is 100% at zero frequency, it abruptly decreases with the frequency and has several peaks at 2.7 eV, 4.7 eV, 5.8 eV, 7.9 eV, and 11.1 eV. Insulator $MnFe_2O_4$ has a small reflectivity (~20%) at zero frequency, and then it increases up to 32% at 3.3 eV and then again decreases with several peaks.

3.2. Inverse structure

Let us consider the properties of the $FeMn_2O_4$ and $MnFe_2O_4$ spinels in the inverse structure. In the inverse spinel structure (Fig. 7), bivalent A-site cations are located in the center of half the octahedron formed by oxygen ions, and trivalent B-site cations are located both in the centers of the other half of the octahedra and in the centers of the oxygen tetrahedra. The lattice parameters of the spinels in the inverse structure are larger than in the normal structure; the magnetic moments are close to the ones in the normal structure(see Table 4). The tendency for the Mn magnetic moment to be larger in the tetrahedral site as compared with the octahedral position and for the magnetic moment of iron to be large in the octahedral position is also preserved. The occupation numbers of

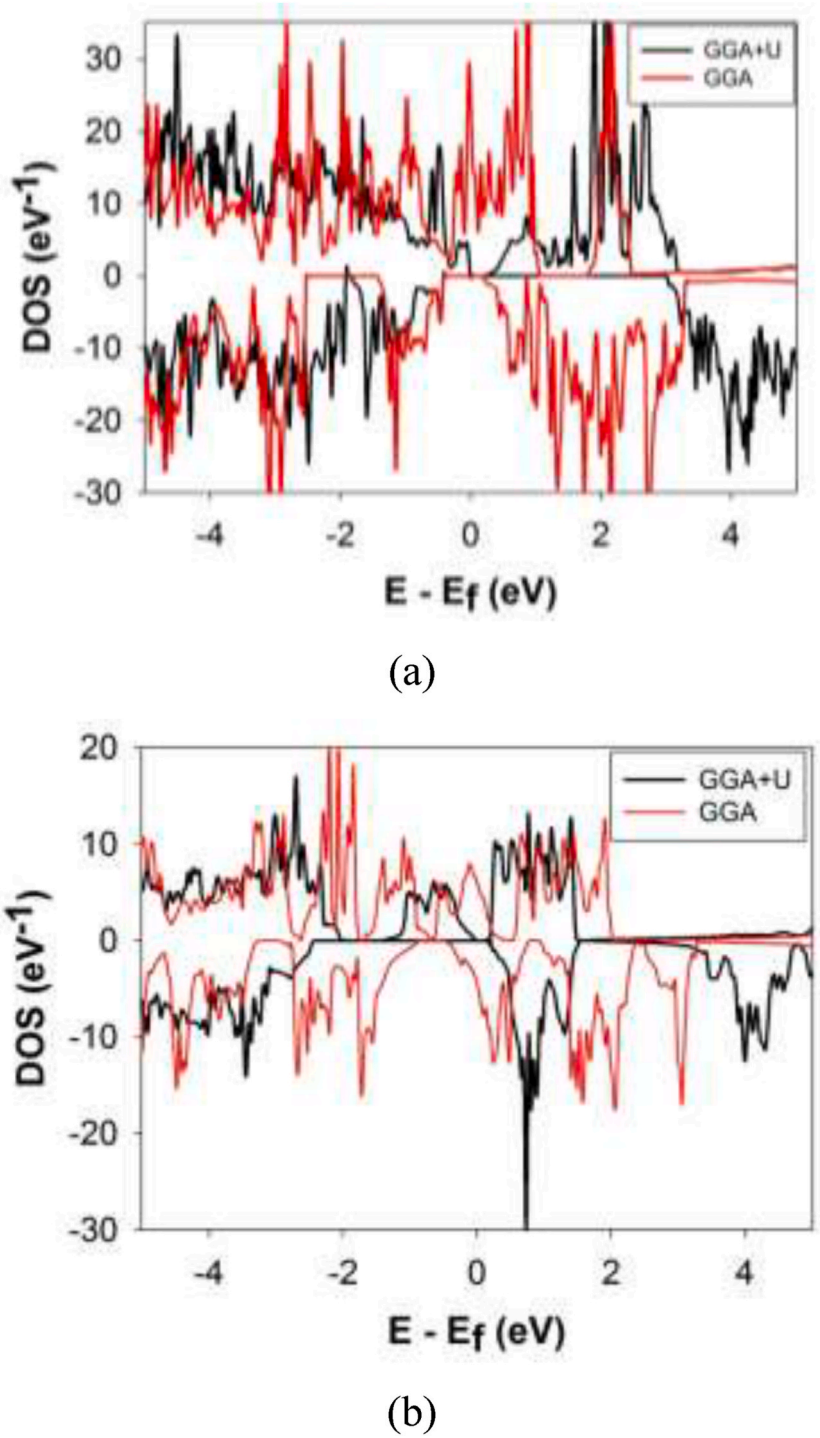

Fig. 8. Total DOS of (a) $FeMn_2O_4$ and (b) $MnFe_2O_4$ inverse spinels. Black line – GGA + U, red line – GGA. The zero on the energy axis is the Fermi energy. Negative values of DOS correspond to the spin-down states. (For interpretation of the references to color in this figure legend, the reader is referred to the Web version of this article.)

the Mn and Fe ions are close to the nominal; therefore, d-electrons of both ions are in high-spin states.

To find a ground state, we have calculated and compared the total energies of cubic and tetragonal structureы of $FeMn_2O_4$ and $MnFe_2O_4$ with different magnetic arrangements of magnetic moments (Table 5). One can see from Table 6 that $FeMn_2O_4$ is the tetragonal crystal, whereas in $MnFe_2O_4$ cubic structure is more favorable by energy. Both compounds are ferrimagnetic, however, the magnetic structures differ. In the inverse $FeMn_2O_4$, the magnetic moments of Mn ions in the A- and half of the B-sites are antiparallel to the magnetic moments of Fe ions on the other half of B-sites. In turn, in the inverse $MnFe_2O_4$, ions in the A-sites (Fe) are antiparallel to the ions in the B-sites (Fe and Mn). The comparison of the ground state energy of the normal and inverse spinels (Tables 3 and 6) shows the preferability of the normal structure for both spinels.

As seen in Fig. 8, in the inverse $MnFe_2O_4$, the energy gap remains; however, its width decrease down to 0.3 eV for the majority-spin channel and down to 2.7 eV for the minority-spin channel as

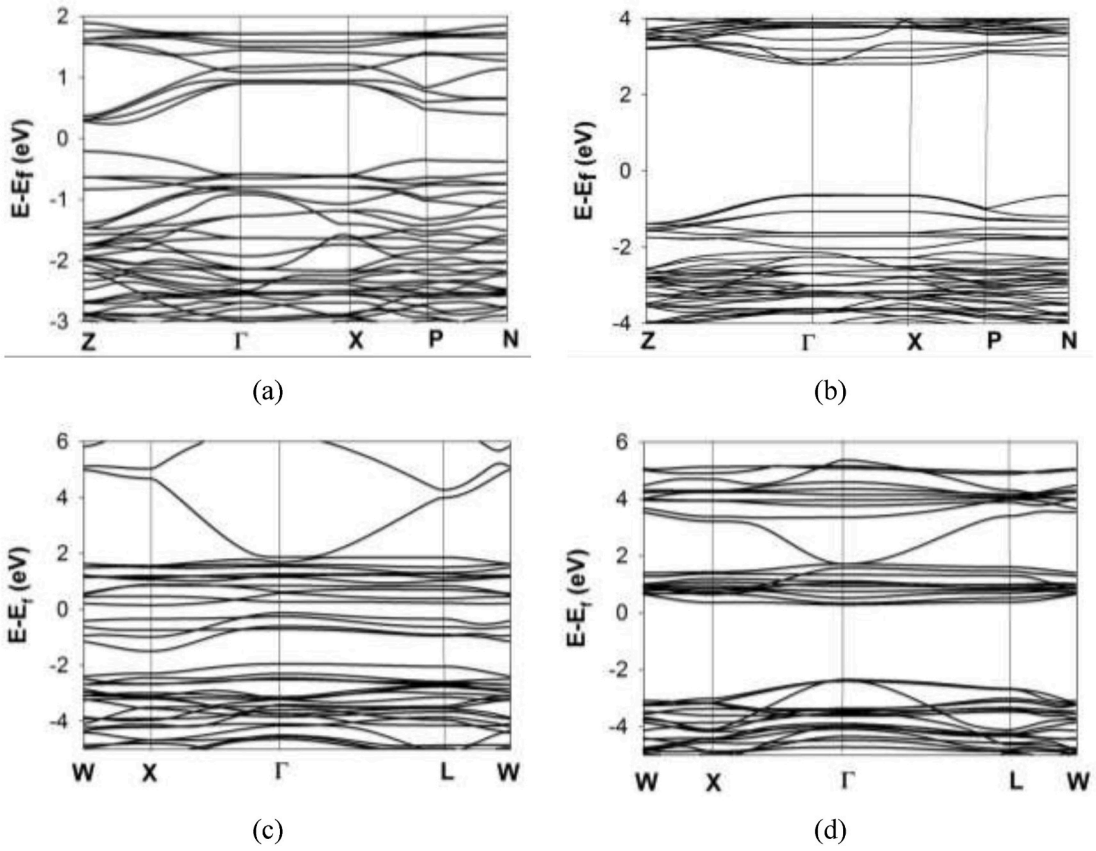

Fig. 9. Band structures of the inverse spinels: (a), (b) –$FeMn_2O_4$, (c), (d) – $MnFe_2O_4$. Zero corresponds to the Fermi energy.

compared with the normal spinel. Interestingly, in $FeMn_2O_4$, the small bandgap opens for the spin-up channel, unlike the metal behavior of the spin-up channel in normal spinel. This fully agrees with experimental results [17]. Notice, that bandgap in inverse $FeMn_2O_4$ appears only for the tetragonal structure.

The comparison of band structures of the inverse $FeMn_2O_4$ and $MnFe_2O_4$ spinels are given in Fig. 9. Both compounds have a bandgap for both majority and minority spin channels. At that, the bandgap for the minority spin channel is larger than for the majority spin channel. In the inverse $MnFe_2O_4$, the first empty majority-spin flat bands (Eg and T2g) are formed by the d-states of tetrahedral Fe ion. The eg-states of Mn form the first valence majority-spin bands. The minority-spin valence and conductive bands nearest to Fermi energy are formed by t2g-states of octahedral Fe ions and t2g-states of Mn, correspondingly, with a significant admixture of p-states of O. The behavior of minority-spin band structure of inverse $FeMn_2O_4$ is similar to one in the normal spinel. However, the majority-spin band structure differs. In the inverse spinel, the valence band formed by d-electrons of tetrahedral manganese ion and p-electrons of oxygen are separated by an energy gap from the empty bands formed by t2g-states of octahedral manganese ions and t2g-states of the iron ions. In the part of the Brillouin zone, the spin-up gap width is about 1.75 eV; however, in the Γ-Z and X-P-N directions, it narrows down to 0.5–0.7 eV.

In the inverse spinel, there are two superexchange constants between tetrahedral and octahedral ions: between identical and between different species in A and B-sites. The expressions for the exchange integrals between A- and B-site cations within the indirect coupling model have the following forms for $FeMn_2O_4$ and $MnFe_2O_4$ inverse spinels, correspondingly:

$$J_{Mn-Mn} = -\frac{1}{30}a\left\{\left(b\left(U_{Mn}+U_{Fe}-J_{Mn}^{6H}\right)+3c(U_{Mn}+U_{Fe})\right\}\right. \quad (3)$$

$$J_{Mn-Fe} = -\frac{4}{75}a(2b+3c)U_{Fe} \quad (4)$$

$$J_{Fe-Mn} = -\frac{1}{24}a\left\{\left(b\left(U_{Mn}+U_{Fe}-J_{Mn}^{6H}\right)+3c(U_{Mn}+U_{Fe})\right\}\right. \quad (5)$$

$$J_{Fe-Fe} = -\frac{1}{30}a(2b+3c)U_{Fe} \quad (6)$$

where $U(Mn^{2+}) = 7$ eV, U $(Fe^{2+}) = 6.5$ eV, U $(Mn^{3+}) = 8.5$ eV and U $(Fe^{3+}) = 8$ eV are the cation-ligand excitation energy; a, *b* and *c* are the electron transfer parameters being squares of A and B ligand-cations intermixing coefficients for the σ and π coupling, respectively (the values of these parameters are $a = 0.08$, $b = 0.02$ and $c = 0.01$); $J_{Mn}^{6H} = 3$ eV – intraatomic exchange integral [16–18]. The calculated exchange integrals are $J_{Mn\text{-}Mn} = -1{,}97$ meV (~22 K), $J_{Mn\text{-}Fe} = -2{,}38$ meV (~26 K) for $FeMn_2O_4$ and $J_{Fe\text{-}Mn} = -2{,}38$ meV (~26 K), $J_{Fe\text{-}Fe} = -2{,}7$ meV (~30 K) for $MnFe_2O_4$ spinel, correspondingly. One can see that Fe–Mn superexchange integrals in both compounds are also antiferromagnetic in agreement with the results of our ab initio calculations and experimental data [32], and their values are close to the ones in the normal spinels. The exchange constants between different A-B couplings are larger than exchange constants of the between the same A-B couplings.

4. Conclusions

In conclusion, we have performed the calculation, comparison, and analysis of magnetic, electronic, and optical properties of the spinels $MnFe_2O_4$ and $FeMn_2O_4$ in two structural types: normal spinel and inverse spinel. In both structures, the compounds are ferrimagnetic, with the large magnetic moments (μ~4–4.5 μ_B) on magnetic ions. The inverse spinel is less favorable by energy than the normal one. The structural and electronic properties of spinels differ depending on the cations on A-

and B-sites. The normal $FeMn_2O_4$ spinel has the tetragonal structure with the half-metal properties; however, in the inverse $FeMn_2O_4$, the small energy gap opens. At the same time, $MnFe_2O_4$ is the insulator with the cubic structure. Energy gap changes from about E_g ~1.5 eV in normal spinel to an about E_g ~0.5 eV in inverse spinel. The calculated exchange integrals are close to the experimental ones, and they are weak for both spinels due to the superexchange couplings of magnetic species. The magnetic moment of the octahedral Mn ion in $FeMn_2O_4$ has a pronounced dependence on the hydrostatic pressure which leads to its sharp drop and, as a consequence, a sharp decrease in the total magnetization when a pressure above 60 GPa is applied. The absorption and reflection spectra of the $MnFe_2O_4$ and $FeMn_2O_4$ spinels are also differed due to the difference in the electronic structure.

CRediT authorship contribution statement

V.S. Zhandun: Conceptualization, Methodology, Validation, Software, Investigation, Writing - review & editing, Supervision. **A.V. Nemtsev:** Software, Investigation, Writing - original draft.

Declaration of competing interest

The authors declare that they have no known competing financial interests or personal relationships that could have appeared to influence the work reported in this paper.

Acknowledgments

The reported study was funded by Russian Foundation for Basic Research, Government of Krasnoyarsk Territory, Krasnoyarsk Regional Fund of Science to the research project № 19-42-240016: «Control of structural, magnetic, electronic, and optical properties by pressure and intercalation into functional compounds with a spinel structure containing 3d and 4f ions » The calculations were performed with the computer resources of "Complex modeling and data processing research installations of mega-class" SRC "Kurchatovsky Institute" (http://ckp.urcki.ru).

References

[1] V.W.J. Verhoeven, F.M. Mulder, I.M. De Schepper, Phys. B (Amsterdam, Neth.) 276–278 (2000) 950.
[2] V. Kocsis, S. Bordács, D. Varjas, K. Penc, A. Abouelsayed, C.A. Kuntscher, K. Ohgushi, Y. Tokura, I. Kézsmárki, Phys. Rev. B 87 (2013), 064416.
[3] V. Fritsch, J. Hemberger, N. Büttgen, E.-W. Scheidt, H.-A. Krug von Nidda, A. Loidl, V. Tsurkan, Phys. Rev. Lett. 92 (2004) 116401.
[4] R. Fichtl, V. Tsurkan, P. Lunkenheimer, J. Hemberger, V. Fritsch, H.-A. Krug von Nidda, E.-W. Scheidt, A. Loidl, Phys. Rev. Lett. 94 (2005), 027601.
[5] D. Santos-Carballal, A. Roldan, R. Grau-Crespo, N.H. de Leeuw, Phys. Rev. B 91 (2015) 195106.
[6] U. Lüders, A. Barthélémy, M. Bibes, K. Bouzehouane, S. Fusil, E. Jacquet, J.-P. Contour, J.-F. Bobo, J. Fontcuberta, A. Fert, Adv. Mater. 18 (2006) 1733.
[7] A.J. Heeger, T.W. Houston, Phys. Rev. 135 (1964) A661.
[8] B. Boucher, R. Burl, M. Perrin, J. Appl. Phys. 40 (1969) 3.
[9] Xu Zuo, Carmine Vittoria, Phys. Rev. B 66 (2002) 184420.
[10] Mohd Mohsin Nizam Ansari, Shakeel Khan, Naseem Ahmad, J. Magn. Magn Mater. 465 (2018) 81–87.
[11] C. William, Mackrodt, Simson Elizabeth-Ann, J. Chem. Soc., Faraday Trans. 92 (12) (1996) 2043–2048.
[12] U. Koenig, G. Chol, J. Appl. Crystallogr. 1 (1968) 124.
[13] R. Nepal, Q. Zhang, S. Dai, W. Tian, S.E. Nagler, R. Jin, Phys. Rev. B 97 (2018), 024410.
[14] J.-R. Huang, C. Cheng, J. Appl. Phys. 113 (2013), 033912.
[15] J.M. Hastings, L.M. Corliss, Phys. Rev. 104 (1956) 328.
[16] G.A. Sawatzky, F. Van Der Woude, A.H. Morrish, Phys. Rev. 187 (1969) 747.
[17] J.A. Kulkarni, V.S. Darshane, Thermochim. Acta 93 (1985) 473.
[18] V.A.M. Brabers, Phys. Status Solidi 33 (1969) 563.
[19] G. Kresse, J. Furthmüller, Phys. Rev. B 54 (1996) 11169.
[20] P.E. Blochl, Phys. Rev. B 50 (1994) 17953. G. Kresse and D. Joubert, Phys. Rev. B. 59, 1758 (1999).
[21] J.P. Perdew, K. Burke, M. Ernzerhof, Phys. Rev. Lett. 77 (1996) 3865.
[22] H.J. Monkhorst, J.D. Pack, Phys. Rev. B 13 (1976) 5188.
[23] S.L. Dudarev, G.A. Botton, S.Y. Savrasov, C.J. Humphreys, A.P. Sutton, Phys. Rev. B 57 (1998) 1505.
[24] E. Sasıoglu, C. Friedrich, S. Blügel, Phys. Rev. B 83 (R) (2011) 121101.
[25] U. Koenig, G. Chol, J. Appl. Crystallogr. 1 (1968) 124.
[26] A.M. Jacintha, A. Manikandan, K. Chinnaraj, S.A. Antony, P. Neeraja, J. Nanosci. Nanotechnol. V 15 (2015) 9732–9740.
[27] M.L. Néel, Ann. Phys. 12 (1948) 137.
[28] O.A. Bayukov, A.F. Savitskii Fiz, Tverd. Tela 36 (7) (1994) 1923.
[29] P.W. Anderson, Phys. Rev. 115 (1) (1959) 2.
[30] G.A. Sawatzky, W. Geertsma, C. Haas, J. Magn. Magn Mater. 3 (1976) 37.
[31] V.C. Rakhecha, L.M. Rao, N.S.S. Murthy, B.S. Srinivasan, Phys. Lett. 40A (1972) 101.
[32] W. Wegener, D. Scheerlinck, E. Legrand, S. Hautecler, Solid State Commun. 15 (1974) 345.